Numerical computations of cardiac AP using level set based geometries

Myriam Rioux[1,2], Yves Bourgault[1,2], Youssef Belhamadia[3,2], and Olivier Rousseau[1]

[1]Dept. of Mathematics and Statistics, University of Ottawa, ON, Canada. [2]GIREF, Université Laval, QC, Canada.

[3]Mathematics Department, Campus Saint-Jean, University of Alberta, AB, Canada.

***Abstract*—This article proposes two avenues to help improve the realism of numerical computations for cardiac electrophysiology while maintaining manageable computational resources. We first propose an asymptotic analysis to adjust the parameters and use a simple two-variable ionic model to reproduce the main characteristics of the cardiac action potential (AP) in various myocardial regions. This ionic model is embedded in the bidomain model that is used to propagate the AP in the heart. Our second contribution is a finite element method that couples the heart with the torso in a single variational formulation and allows non body fitted meshes at the interface between the myocardium and the torso/ventricle cavities. This interface is described through a level-set function obtained from the segmentation of patient medical images. Using a 2D test case, we compare the use of body-fitted and non body-fitted meshes and analyze the impact of both approaches on the accuracy of the solutions, including an anisotropic mesh adaptation strategy.**

I. Introduction

Non-invasive techniques to image and visualize human tissues can be used to recover patient-specific geometries of organs such as the heart. It would be interesting to use such geometries to do more realistic numerical simulations in cardiac electrophysiology. A main impediment for using these geometries with the current finite element methods solving mono/bidomain models is the inherent complexity of their boundaries and the difficulty of generating conformal meshes over these. Level-set methods that are the basis of several image segmentation methods provide a natural setting for recovering and describing complex geometries. They are also very efficient at simulating physical phenomena with evolving interfaces, such as in free surface fluid mechanics where the fluid domain changes at every time step [11], [10], [18], [9]. In computational electrocardiology, the same need occurs for patient specific simulations, where a new geometry has to be constructed for each patient. For the electromechanical coupling problem, where the myocardium moves in response to an electrical stimulus and fiber contraction, the domain describing the heart changes at each time step.

The goal of the present paper is to develop a finite element method and meshing strategies to handle complex geometries described by level set functions, whose level set functions have been obtained through medical image segmentation. Our finite element method can solve the heart-torso coupling electrophysiological problem. The results of numerical simulations on body fitted meshes are compared with simulations on non body fitted meshes with a level set description of the domains. The aim of this work is to show that one can avoid the step of generating a body fitted mesh, and still have good accuracy when mesh adaptation is used. We concentrate here on a feasibility study in 2D, but the approach is applicable in 3D. Indeed all our computational codes work both for 2D and 3D images and meshes. Meanwhile, we will explain how we managed to keep the model as simple and computations as affordable as possible through the use of a two-variable ionic model calibrated by an asymptotic analysis.

II. Modeling "physiological" action potentials with a two-variable ionic model

A first crucial step in setting computations in cardiac electrophysiology consists in choosing an appropriate ionic model, which is a system of ODEs able to reproduce the shape of the action potential (AP) through time. The Mitchell-Schaeffer (MS) model first introduced in [7] is used in our numerical simulations for the following reasons. Because it is derived from the Fenton-Karma ionic model, it has benefits of a physiological ionic model though it is a phenomenological model. Moreover, many authors have used of the MS model for realistic clinical applications (see for instance [5], [13], [14]).

The activation of the potential in the heart and the propagation of the potential (heart/torso) is modelled through the bidomain model coupled with the MS ionic model:

$$\frac{\partial v}{\partial t} = g(u,v) \quad \text{in } H, \quad (1)$$

$$\frac{\partial u}{\partial t} + I_{ion}(u,v) = \nabla \cdot (N_i \nabla (u + u_e)) \quad \text{in } H, \quad (2)$$

$$\nabla \cdot (\sigma_i \nabla u) + \nabla \cdot ((\sigma_i + \sigma_e) \nabla u_e) = 0 \quad \text{in } H, \quad (3)$$

$$n_H \cdot (\sigma_i \nabla u + (\sigma_i + \sigma_e) \nabla u_e) = n_H \cdot (\sigma_T \nabla u_T) \quad \text{on } \partial H, \quad (4)$$

$$n_H \cdot (\sigma_i \nabla u_i) = 0 \quad \text{on } \partial H, \quad (5)$$

$$\nabla \cdot (\sigma_T \nabla u_T) = 0 \quad \text{in } T, \quad (6)$$

$$n_T \cdot (\sigma_T \nabla u_T) = 0 \quad \text{on } \partial T, \quad (7)$$

where

$$I_{ion}(u,v) = \frac{1}{\tau_{in}} v u^2 (u-1) + \frac{1}{\tau_{out}} u; \quad (8)$$

$$G(u,v) = \begin{cases} \frac{1}{\tau_{open}}(1-v) & \text{for } u < u_{gate}, \\ -\frac{1}{\tau_{close}} v & \text{for } u \geq u_{gate}, \end{cases} \quad (9)$$

978-1-4244-8281-8/11/$26.00 ©2011 IEEE

v is the recovery variable; u_i, u_e and $u = u_i - u_e$ are, respectively, the intracellular, extracellular and transmembrane potentials; σ_i and σ_e are, respectively, the intracellular and extracellular conductivity tensors. The bidomain model is nondimensionalized with characteristic time and space scales T and L, and the nondimensional number $N_i = T\sigma_i/C_m\chi L^2$ is introduced, with χ the cell membrane surface to volume ratio and C_m is the specific capacitance (per unit area) of the cell membrane. The parameters τ_{in}, τ_{out}, τ_{open} and τ_{close} represent time scales in the ionic model. The threshold u_{gate} allows a switch of time scales in the MS model.

A. Asymptotic analysis for setting model parameters

In the human heart, there are different tissues with APs propagating at different speeds and with different wave shapes (meaning AP duration, length of repolarization, refractory periods, etc). Being able to model these various APs is a major endeavor given the complexity of current physiological ionic models. Using a simple and unique ionic model with properly tuned parameters would be a major asset, leading to potentially very efficient computations of realistic APs in the whole heart. Along these lines, we are proposing to choose all parameters of the bidomain and MS models through an asymptotic analysis. This analysis allows on the one hand to propagate the AP at the right speed, and on the other hand to give an appropriate shape to the AP wave. The details are voluntarily omitted here, and the reader is referred to the following papers [16], [17], [19] for a partial derivation of these results.

The first step of the asymptotic analysis is to recover the desired time scales of the AP, illustrated in figure 1. The AP is

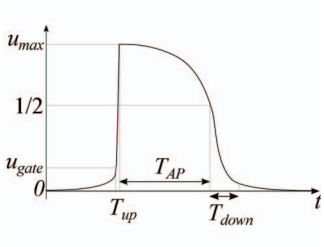

Figure 1. The AP through time measured at a point.

divided in four phases, the depolarization, the excited phase, the repolarization and the recovery, with respective durations T_{up}, T_{AP}, T_{down} and T_{rec}. The following equations relate the time scales τ of the ionic model to the four times scales of the AP:

$$T_{up} = -\frac{k_{up}}{F_{AB}}(u_{max} - u_{gate})^2, \tag{10}$$

$$T_{AP} = \tau_{close} \ln\left(\frac{\tau_{out}}{4\tau_{in}}\right), \tag{11}$$

$$T_{down} = 12 k_{down} \tau_{out}, \tag{12}$$

$$T_{rec} = \tau_{open} \ln\left(\frac{\frac{4\tau_{in}}{\tau_{out}} - 1}{v_{pace} - 1}\right), \tag{13}$$

with

$$F_{AB} = \frac{1}{\tau_{in}}\left(\frac{u_{max}^4}{4} - \frac{u_{max}^3}{3}\right) + \frac{1}{2}\frac{u_{max}^2}{\tau_{out}}$$

Table I
PARAMETERS TO MODEL THE AP OF A VENTRICLE.

Phase	Durations (ms)	MS parameters (ms)		T (ms)
Depol.	8	τ_{in}	0.3150	7.9750
Exc.	250	τ_{close}	168.50	260.93
Repol.	30	τ_{out}	5.5556	31.196
Rec.	260	τ_{open}	94.942	257.41
Phase	Speed (m/s)	Bidomain parameter (nondimensional)		c (m/s)
Depol.	0.5	N	1.8508e-04	0.4368

and

$$u_{max} = \frac{1}{2} + \frac{1}{2}\sqrt{1 - 4\frac{\tau_{in}}{\tau_{out}}}.$$

The constants k_{up} and k_{down} result from approximations done in the asymptotic analysis and were set to 2.15 and 0.45, respectively. The parameter $v_{pace} < 1$ determines the value of the recovery potential v at which the next wave is paced. The application

$$(\tau_{in}, \tau_{out}, \tau_{open}, \tau_{close}) \rightarrow (T_{up}, T_{AP}, T_{down}, T_{rec})$$

is bijective as long as $\tau_{out} > 4\tau_{in}$. It is an important result allowing the selection of the model parameters to match durations of the various AP.

The second step is to impose the speed of propagation by fixing the group of parameters $\sigma/(C_m\chi)$ in the bidomain model using

$$c = -k_c\sqrt{\frac{\sigma}{C_m\chi}}\frac{F_{AB}\sqrt{T_{up}}}{(u_{max} - u_{gate})^2}. \tag{14}$$

with $k_c = 2.95$, a value adjusted for good predictions.

This asymptotic analysis allows the computation of the restitution curves for the upstroke duration, the action potential duration, the downstroke duration and the speed versus the last recovery duration. Shaping a single wave as well as sequences of waves reduces in straightforward function evaluations. Other properties characterizing the AP wave can be extracted from the asymptotic solution like the maximal rate of depolarization dV/dt_{max}. Details will be given in a forthcoming paper.

Any characteristic time T and length L can be chosen as long as these are consistent with the domain dimensions. For instance, if a numerical simulation is done on a mesh of a human heart, L has to be fixed so that the heart has the right dimension and T can be chosen arbitrarily. The nondimensional values of τ's in the MS model will have to be adjusted consequently because the original MS model is designed for $T = 1$ ms.

When using $T = 1$ ms and $L = 1$ mm for a simple 1D numerical simulation, if the values of the second column of Table I are desired for the numerical solution, the parameters of the fourth column are found using the asymptotic analysis. The last column shows the values measured on the numerical solution, highlighting the efficiency of the asymptotic method.

III. Finite element methods on level-set domains

We propose a new finite element method for solving the heart-torso coupling problem using non body fitted meshes and a level set description of the domains. We first present the finite element method then discuss issues related to meshes and level set functions.

A. Variational formulation and finite element method

The heart-torso coupling problem given by Eq. (1)-(7) with the ionic model given by Eq. (8)-(9) is now rewritten as a standard Galerkin formulation and solved using a finite element method. Under the assumption that the solution is sufficiently regular the following variational formulation is obtained:

$$\int_H \frac{dv}{dt}\phi_v + \int_H g(u,v)\phi_v = 0$$

$$\int_H \frac{du}{dt}\phi_u + \int_H N_i\nabla(u+u_e)\cdot\nabla\phi_u + \int_H f(u,v)\phi_u = \int_{\partial H}(N_i\nabla(u+u_e))\cdot n_H\phi_u$$

$$\int_H \sigma_i\nabla u\cdot\nabla\phi_w + \int_H(\sigma_i+\sigma_e)\nabla u_e\cdot\nabla\phi_w = \int_{\partial H}(\sigma_i\nabla u + (\sigma_i+\sigma_e)\nabla u_e)\cdot n_H\phi_w$$

$$\int_T \sigma_T\nabla u_T\cdot\nabla\phi_w = \int_{\partial T\cap\partial H}\sigma_T\nabla u_T\cdot n_T\phi_w + \int_{\partial T-\partial T\cap\partial H}\sigma_T\nabla u_T\cdot n_T\phi_w.$$

The variational formulation above cannot be used in its current form due the presence of the normal derivatives on the boundaries ∂T and ∂H. Moreover, the solutions of the problems on the heart and the thorax must be coupled. To solve these issues, we use the boundary conditions (4), (5) and (7), and define the following new quantities:

$$\sigma_w = \begin{cases}\sigma_i+\sigma_e & \text{in } H\\ \sigma_T & \text{in } T\end{cases}$$

$$\widetilde{\sigma_i} = \begin{cases}\sigma_i & \text{in } H\\ 0 & \text{in } T\end{cases}$$

$$u_w = \begin{cases}u_e & \text{in } H\\ u_T & \text{in } T.\end{cases}$$

We get a new variational formulation that couples subdomain problems and solves the issue with Neumann and transmission boundary conditions:

$$\int_H \frac{ds}{dt}\phi_v + \int_H g(s,u,t)\phi_v = 0 \tag{15}$$

$$\int_H \frac{du}{dt}\phi_u + \int_H N_i\nabla(u_w|_H)\cdot\nabla\phi_u + \int_H N_i\nabla u\cdot\nabla\phi_u + \int_H f(s,u)\phi_u = 0 \tag{16}$$

$$\int_{H\cup T}\widetilde{\sigma_i}\nabla u\cdot\nabla\phi_w + \int_{H\cup T}\sigma_w\nabla u_w\cdot\nabla\phi_w = 0 \tag{17}$$

Functional spaces must be set for this variational problem to be well-posed. We seek a unique weak solution $v \in L^2(0,T;L^2(H))$, $u \in L^2(0,T;H^1(H))$, $u_w \in \{v \text{ s.t. } v|_H \equiv u_e \in L^2(0,T;H^1(H)/\mathbb{R}), v|_T \equiv u_T \in L^2(0,T;H^1(T)/\mathbb{R}), u_e|_{\partial H} = u_T|_{\partial H}\}$. Note that the transmission condition (4) is naturally enforced by this variational formulation.

This variational formulation can be discretized in space for instance using continuous P_k finite elements and in time using a time-stepping scheme. The time-stepping scheme chosen is the implicit Gear or BDF2 scheme (investigated and used in [8] and [3]) which has the merit to be second order in time and stable for relatively large time steps. We did not investigate more about the time discretization, but we rather focussed on the space discretization using appropriate meshing strategies.

B. Level set description of the domain and issues related to meshes

A level set function is defined as follows:

Definition 1. If Ω is the whole domain, H defines the heart subdomain, the level set description of the heart is defined through a continuous function $\varphi : \Omega \to \mathbb{R}$ such that

$$\varphi(x)\begin{cases}<0 & \text{for } x\in H,\\ =0 & \text{for } x \text{ on } \partial H,\\ >0 & \text{otherwise.}\end{cases} \tag{18}$$

The level curve $\varphi = 0$ represents the interface ∂H.

Figure 2 illustrates three approaches for handling internal boundaries such as the heart-torso interface. The simplest situation occurs with polygonal interface that can be exactly discretized with linear triangular meshes. Curved boundaries, as obtained through level set description, can be handled either by enforcing mesh vertices to stand on the boundary (so called "body fitted" meshes) or without any restriction on the vertices near the boundary ("non body fitted" meshes).

(a) Body fitted mesh, polygonal domain. (b) Body fitted mesh, domain with a curved boundary. (c) Non body fitted mesh.

Figure 2. Body fitted meshes vs a non body fitted mesh. The internal interface is in red.

The approach proposed here uses realistic geometries coming from segmented medical images. Figure 3(a) represents a high resolution CT scan, courtesy of the Ottawa Heart Institute. The CT scan has size $512 \times 512 \times 199$ pixels and a horizontal resolution of 0.49×0.49 mm. This image is a horizontal slice of the original three-dimensional CT scan exhibiting a cut through the two cardiac ventricles as well as a fraction of the lungs. The heart geometry shown on fig. 3(b)

was extracted from this CT scan. This image segmentation was performed using a variant of the Chan-Vese method [6]. Details on the segmentation methodology are given in [15]. The segmentation provides a level set function describing the boundaries between the myocardium and the torso and the ventricle cavities. Body-fitted meshes were obtained using *DistMesh* [12], a mesher well suited for domains implicitly defined with level set functions. Non body fitted meshes are easily obtained with any mesher that generates regular grids. Figure 3(c) shows a relatively coarse regular mesh obtained with this second approach.

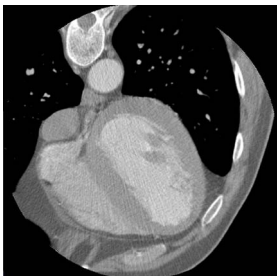

(a) Medical image. Source: University of Ottawa Heart Institute.

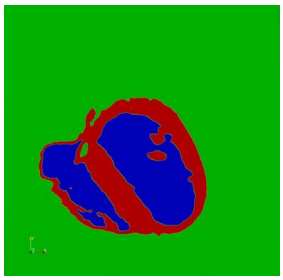

(b) Segmentation.

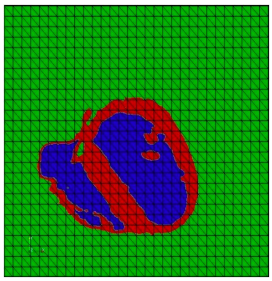

(c) Non body fitted mesh.

Figure 3. Preliminary steps of a realistic simulation with non body fitted meshes: From a medical image (a), a segmentation (b) is done to capture the complicated internal interfaces. A simple (non body fitted) mesh (c) is built on the whole image.

Once the segmentation of the medical image is done and the whole domain is triangulated with a non body-fitted mesh, the problem has to be solved efficiently using a level set description of the domains. The variational formulation (15)-(17) is not directly applicable because the domains H and T are not yet defined as sets of elements. One way to tackle the problem is to defined the heart domain as the largest set of elements which fit completely inside the level set description of the heart (see fig. 4). A signed distance function is used as level set function to achieve this task.

C. The need of mesh adaptation

The numerical simulations in cardiac electrophysiology are known to require extremely fine meshes in order to capture all phenomena initiated by the ionic model. If great computational resources are available, parallel computing techniques can be used on a fixed mesh. Attempting to address this problem in a different way, a mesh adaptation strategy can improve performance and accuracy as well. Anisotropic mesh adaptation has already been used for numerical simulations in cardiac

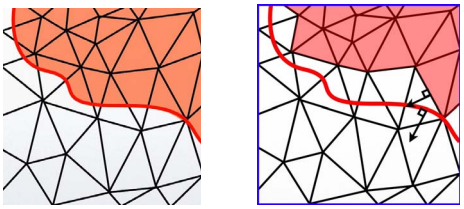

Figure 4. Left: The heart domain defined by a level set is in red. Right: The heart domain defined as the largest set of elements which fit completely inside the level set description of the heart.

electrophysiology based on the monodomain model in the heart only (see [4]). The method proposed was shown to be far superior in terms of performance and accuracy to uniform mesh methods commonly used in cardiac electrophysiology especially over realistic heart geometries.

A similar strategy is employed here and the mesh is adapted to minimize the error on the solution (u, v, u_w). The mesh adaptation is based on a metric which depends on the second derivatives of the numerical solution (see [1], [2] for more details). The mesh is updated at each time step.

Given that geometries are handled through a level set description in the current work, much care is required. The problem (15)-(17) naturally imposes the transmission conditions (4). However, when it is solved on a non body fitted mesh there could be a bad approximation of the normal vector when the mesh is coarse (see fig. 4). To keep as precise as possible the definition of the domains, the mesh is refined and aligned in the neighborhood of internal interfaces. In particular non body fitted meshes greatly simplifly the handling of internal boundaries while using anisotropic adaptation to reach the highest accuracy of the finite element method and avoid spurious excitations near these interfaces. Our goal here is precisely to show that electrophysiological waves can be propageted on non body fitted meshes over the heart and thorax with the same accuracy as on body fitted meshes but in a much easier way if anisotropic mesh adaptation is used.

IV. Results

We now present the AP computed on the geometry illustrated on fig. 3(c). The AP is initiated with a localized super-threshold region near the lower junction of the septum and the cardiac walls. Figure 5 illustrates the solution at time step 275 over a non body fitted mesh ($\Delta t = 0.3$ ms) with realistic fiber arrangement. The parameters of the models are given in table I together with $u_{gate} = 0.13$, $C_m = 0.01$ F/m^2, $\chi = 2 \times 10^5$ m^{-1}, $\sigma_{i,t} = 0.6964$, $\sigma_{i,n} = 0.07736$, $\sigma_{e,t} = 1.5624$, $\sigma_{i,n} = 0.788$, $\sigma_T = 0.88$, with the indices t and n referring respectively to the tangent and normal fiber directions.

To quantify the accuracy of this time-dependant problem, we have to find a way to compare the solutions for body fitted versus non body fitted simulations. We proceed by comparing the isochrons of depolarization iso_{depol}. These are computed as the first time each node x_i of the mesh is depolarized, i.e the transmembrane potential u crosses from below the threshold $u_{gate} = 0.13$. For plotting isochron contours, the

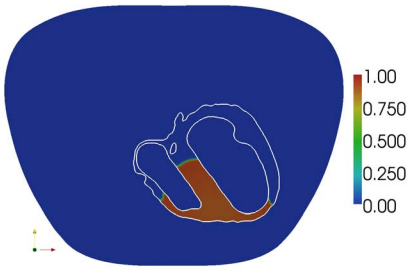

(a) The nondimensional transmembrane potential u.

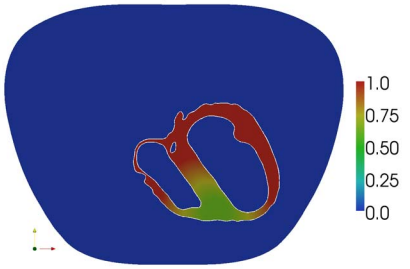

(b) The nondimensional recovery variable v.

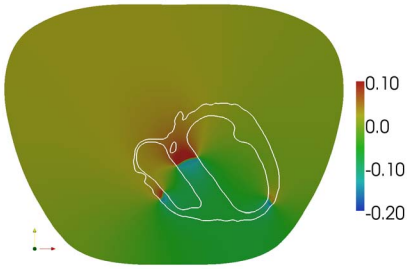

(c) The nondimensional extracellular and torso potential $u_w|_H = u_e$ and $u_w|_T = u_T$.

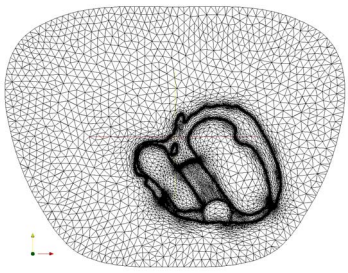

(d) Adapted mesh.

Figure 5. The solution (u, v, u_w) and the mesh at time $t = 82.5$ ms for the non body fitted simulation.

nodal iso_{depol} are interpolated using P_1 shape functions on a background mesh of meshsize $h \sim 3$ mm (twice the front displacement during a time step of 0.3 ms).

Figure 6(a) shows contours of the isochrons of both the body and non body fitted simulations. As mentioned in Sec. III-C

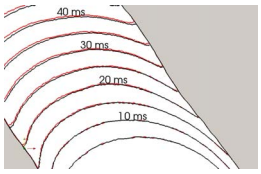

(a) Contours of the depolarization isochrons. Black contours: non body fitted mesh. Red contour: body fitted mesh.

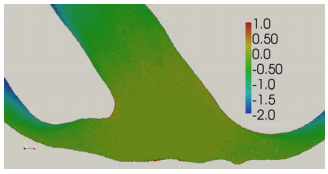

(b) Difference (in ms) between the isochrons of depolarization for the body and the non body fitted mesh.

Figure 6. Difference between the isochrons of depolarization for the body and the non body fitted mesh for the first 65 ms.

the AP velocity is likely to exhibit the largest error near the interface ∂H, a consequence of the inaccurate normal vectors that spoil the transmission conditions. Figure 6(b) shows that the difference between the isochrons of non body fitted and body fitted simulations is larger near the interface but the conduction error diffuses from the interface to the interior of the domain. As expected with any time-stepping scheme, the depolarization time lag increases with the number of time steps basically as the wave travels away from the activation zone. Our results indicate a lag of about 10 ms for the complete depolarization of the heart between the body and non body fitted meshes. Fortunately, anisotropic mesh adaptation provides means to control and mitigate this progressive loss of accuracy for non body fitted meshes, for instance by refining and aligning the elements along the interface. This is clearly illustrated on Fig. 7 where mesh elements follow very precisely the interface even in regions with high curvature.

Figure 7. The anisotropic mesh is refined near internal interfaces. The red curve represents the level set $\varphi = 0$ of the distance function φ from the surface of the heart. The domain of the heart (colored in blue) is defined as the largest set of elements completely inside $\varphi \leq 0$. This figure shows a portion of the heart cavity with the largest interface curvature.

V. Conclusion

We proposed a finite element method for computing cardiac AP on non body fitted meshes over a patient specific heart-torso domain described through level set functions. It is possible to control the accuracy of the solution by combining this methodology with anisotropic mesh adaptation. This way of tackling the problem is very promising as the methodology

could easily be extended to moving geometries and deal with a beating heart. It would facilitate significantly the integration of a model combining the conduction and the contraction of the myocardium, an area that is still wide open. Of course, the potential of the method still needs to be investigated for 3D computations.

ACKNOWLEDGEMENTS

This work was supported by a NSERC Discovery Grant, NSERC and FQRNT post-graduate scholarships to the first and fourth authors. Special thanks to the *University of Ottawa Heart Institute* for providing the CT scan data.

REFERENCES

[1] Frédéric Alauzet. Estimateur d'erreur géométrique et métriques anisotropes pour l'adaptation de maillage. Partie I: aspects théoriques. Rapport de recherche INRIA no. 4759, 10 mars 2003.

[2] Frédéric Alauzet. Estimateur d'erreur géométrique et métriques anisotropes pour l'adaptation de maillage. Partie II: exemples d'applications. Rapport de recherche INRIA no. 4789, 31 mars 2003.

[3] Youssef Belhamadia. A time dependent adaptive remeshing for electrical waves of the heart. *IEEE Transactions on Biomedical Engineering*, 55(2):443–452, 2008.

[4] Youssef Belhamadia, André Fortin, and Yves Bourgault. Towards accurate numerical method for monodomain models using a realistic heart geometry. *Mathematical Biosciences*, 220(2):89 – 101, 2009.

[5] M. Boulakia, M. Fernàndez, J.-F. Gerbeau, and N. Zemzemi. Towards the numerical simulation of electrocardiograms. In Frank Sachse and Gunnar Seemann, editors, *Functional Imaging and Modeling of the Heart*, volume 4466 of *Lect. Notes Comput. Sci.*, pages 240–249. Springer Berlin / Heidelberg, 2007.

[6] TF. Chan and LA. Vese. Active contours without edges. *Image Processing, IEEE Transactions on*, 10(2):266–277, 2001.

[7] Tolkacheva EG, Schaeffer DG, Gauthier DJ, and Mitchell CC. Analysis of the Fenton-Karma model through an approximation by a one-dimensional map. *Chaos*, 12:1034–1042, December 2002.

[8] Marc Ethier and Yves Bourgault. Semi-implicit time-discretization schemes for the bidomain model. *SIAM Journal of Numerical Analysis*, 46(5):2443–2468, 2008.

[9] André Fortin and Khalid Benmoussa. An adaptive remeshing strategy for free-surface fluid flow problems. part II: the three-dimensional case. *Journal of Polymer Engineering*, 26(1):59–86, 2006.

[10] Stanley Osher and Ronald P. Fedkiw. Level set methods: An overview and some recent results. *Journal of Computational Physics*, 169(2):463–502, May 2001.

[11] Stanley Osher and James A. Sethian. Fronts propagating with curvature-dependent speed: Algorithms based on Hamilton-Jacobi formulations. *Journal of Computational Physics*, 79:12–49, 1988.

[12] PO. Persson and G. Strang. A Simple Mesh Generator in MATLAB. *SIAM Review*, 46(2):329–345, 2004.

[13] Jatin Relan, Maxime Sermesant, Hervé Delingette, Mihaela Pop, Graham A. Wright, and Nicholas Ayache. Quantitative comparison of two cardiac electrophysiology models using personalisation to optical and MR data. In *Proceedings of the Sixth IEEE International Symposium on Biomedical Imaging 2009 (ISBI'09)*, July 2009.

[14] Jatin Relan, Maxime Sermesant, Mihaela Pop, Hervé Delingette, Michel Sorine, Graham A. Wright, and Nicholas Ayache. Parameter estimation of a 3d cardiac electrophysiology model including the restitution curve using optical and MR data. In *World Congress on Medical Physics and Biomedical Engineering, WC 2009, München*, September 2009.

[15] Olivier Rousseau. *Geometrical Modeling of the Heart*. PhD thesis, University of Ottawa, 2010.

[16] D. Schaeffer, J. Cain, D. Gauthier, S. Kalb, R. Oliver, E. Tolkacheva, W. Ying, and W. Krassowska. An ionically based mapping model with memory for cardiac restitution. *Bulletin Math. Bio.*, 69:459–482, 2007. 10.1007/s11538-006-9116-6.

[17] D. Schaeffer, W. Ying, and X. Zhao. Asymptotic approximation of an ionic model for cardiac restitution. *Nonlinear Dyn.*, 51:189–198, 2008. 10.1007/s11071-007-9202-9.

[18] Mark Sussman, Peter Smereka, and Stanley Osher. A level set approach for computing solutions to incompressible two-phase flow. *Journal of Computational Physics*, 114(1):146–159, September 1994.

[19] Aizik I. Volpert, Vitaly A. Volpert, and Vladimir A. Volpert. Traveling wave solutions of parabolic systems, 1994.